Tunable biaxial in-plane compressive strain in a Si nanomembrane transferred on a polyimide film

Munho Kim, Hongyi Mi, Minkyu Cho, Jung-Hun Seo, Weidong Zhou, Shaoqin Gong, and Zhenqiang Ma

---

Articles you may be interested in
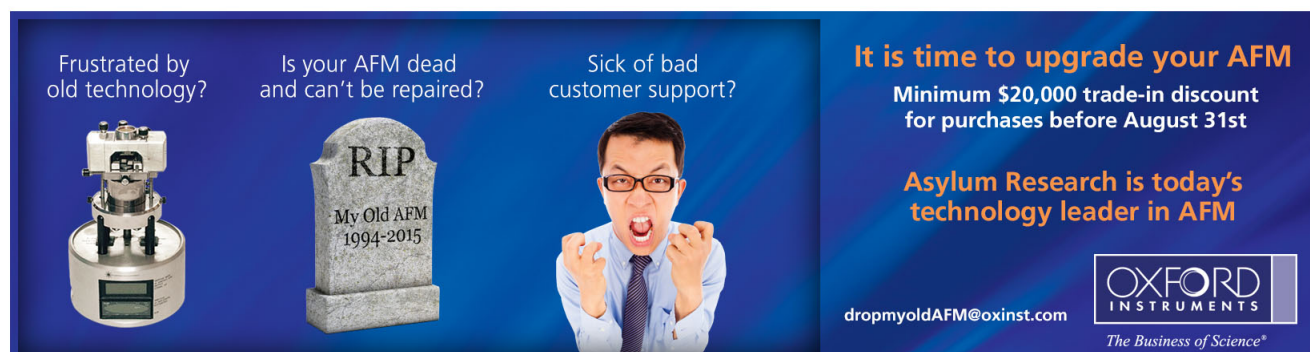
Three dimensional strain distribution of wrinkled silicon nanomembranes fabricated by rolling-transfer technique
Appl. Phys. Lett. **103**, 264102 (2013); 10.1063/1.4857875

In-plane strain distribution in the surface region of thin silicon overlayers on insulator
Appl. Phys. Lett. **86**, 263112 (2005); 10.1063/1.1977208

Roles of hydrogen dilution on the microstructural and optoelectronic properties of B-doped nanocrystalline Si:H thin films
J. Appl. Phys. **95**, 3961 (2004); 10.1063/1.1664028

In-plane strain fluctuation in strained-Si/SiGe heterostructures
Appl. Phys. Lett. **83**, 4339 (2003); 10.1063/1.1629142

In-plane control of morphology and tunable photoluminescence in porous silicon produced by metal-assisted electroless chemical etching
J. Appl. Phys. **91**, 6134 (2002); 10.1063/1.1465123

Tunable biaxial in-plane compressive strain in a Si nanomembrane transferred on a polyimide film

Munho Kim,[1] Hongyi Mi,[1] Minkyu Cho,[1] Jung-Hun Seo,[1] Weidong Zhou,[2] Shaoqin Gong,[3] and Zhenqiang Ma[1,a)]

[1]Department of Electrical and Computer Engineering, University of Wisconsin–Madison, Madison, Wisconsin 53706, USA
[2]Department of Electrical Engineering, University of Texas at Arlington, Arlington, Texas 76019, USA
[3]Department of Biomedical Engineering and Wisconsin Institute for Discovery, University of Wisconsin–Madison, Madison, Wisconsin 53706, USA

A method of creating tunable and programmable biaxial compressive strain in silicon nanomembranes (Si NMs) transferred onto a Kapton® HN polyimide film has been demonstrated. The programmable biaxial compressive strain (up to 0.54%) was generated utilizing a unique thermal property exhibited by the Kapton HN film, namely, it shrinks from its original size when exposed to elevated temperatures. The correlation between the strain and the annealing temperature was carefully investigated using Raman spectroscopy and high resolution X-ray diffraction. It was found that various amounts of compressive strains can be obtained by controlling the thermal annealing temperatures. In addition, a numerical model was used to evaluate the strain distribution in the Si NM. This technique provides a viable approach to forming in-plane compressive strain in NMs and offers a practical platform for further studies in strain engineering. © 2015 AIP Publishing LLC.
[http://dx.doi.org/10.1063/1.4922043]

In recent years, strained silicon (s-Si) has been widely applied to boost carrier mobility in order to achieve a higher drive current in Si-based field-effect transistors (FETs).[1–5] Such strain engineering has been mostly limited to rigid substrates. However, the use of flexible substrates combined with strain engineering enables applications such as flexible sensors and smart patches.[6,7] Although there have been on-going efforts to manipulate the strain in flexible electronics, achieving s-Si on flexible substrates has been a challenge. With the recent advent of transferrable semiconductor nanomembranes (NMs), strain engineering using NMs has received great attention.[8] For example, Yuan et al. first demonstrated the use of tri-layers of single-crystal Si/SiGe/Si NM to obtain s-Si on a plastic substrate.[9] Zhou et al. further utilized the tri-layer Si NM to fabricate flexible RF thin-film transistors (TFTs). They achieved a biaxial tensile strain of 0.35% and an approximately 40% enhancement in electron mobility compared to unstrained devices.[10] Additionally, a unique light-emitting property was obtained from indirect band-gap materials, such as germanium (Ge) NM, by applying biaxial tensile strain.[11] Thus, strain engineering in flexible electronics provides a method to enhance the device performance. However, thus far, strain engineering for flexible electronics usually requires expensive growth equipment, such as a metal organic chemical vapor deposition (MOCVD) system, to grow delicate epitaxial layers.[9,10] Although other methods, such as gas blowing, may also be applicable to flexible substrates, such methods could not yield strain without a use of external forces and using this method only tensile strain can be generated.[11] Therefore, there is a need to develop simpler methods to generate strain on flexible substrates.

Herein, we report a simple and viable method to create programmable biaxial compressive strain in the Si NM using the unique thermal property of Kapton® HN film. Namely, according to the manufacturer's data sheet, the Kapton HN film shrinks when exposed to constant heat due to the residual stress generated in the film during its manufacturing process.[12] The Kapton HN film's unique thermal property allows for the creation of tunable and programmable compressive strains in the film (e.g., Si NM) attached on the top of the Kapton HN film through an annealing process. We investigated the correlation between the amount of strain and the annealing temperature using Raman spectroscopy and high resolution X-Ray diffraction (HR-XRD). We also created a numerical model using a COMSOL Multiphysics® simulation software to analyze the strain distribution in Si NM after the complete annealing process.

Figure 1 schematically illustrates the process of the development of biaxial in-plane compressive strain in Si NMs attached on the top of the Kapton HN films. The creation of strained Si NMs began with a thorough cleaning of the silicon on-insulator (SOI) wafer (with a 200 nm thick top Si (100) layer doped with boron at a concentration of $1.0 \times 10^{15} \, \text{cm}^{-3}$) with acetone, IPA, and DI water. After the top Si layer was photolithographically defined, the SOI samples were undercut in a concentrated hydrofluoric acid (HF, 49%) solution as reported elsewhere.[13] Then, the released top Si layer, now called Si NM, was flip-transferred onto a 125 μm thick Kapton HN film coated with an 1 μm thick adhesive layer (Microchem, SU-8 2002). Transferred Si NMs (size: $2 \times 1.5 \, \text{mm}^2$) were completely glued to the Kapton HN films by following a UV curing process.[14] The samples were annealed at different temperatures in the vacuum chamber with a nitrogen ambient. During the annealing process, the samples were heated to the set temperature at a heating rate

a)Author to whom correspondence should be addressed. Electronic mail: mazq@engr.wisc.edu
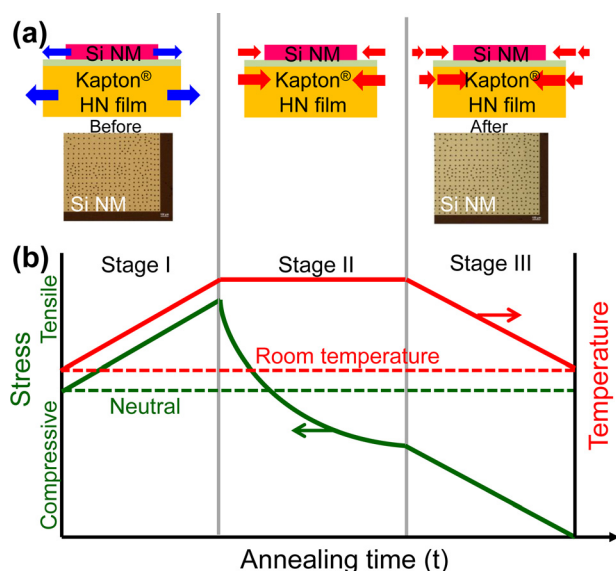
(a)

(b)

FIG. 1. (a) Schematic illustration of the mechanism for the creation of the programmable biaxial compressive strain in a Si NM on a Kapton HN film using the thermal annealing process. During the heating process (stage I), transferred Si NM is under a tensile stress due to the expansion of the Kapton HN film (stage I). During the annealing process (stage II), the tensile stress in the Si NM is decreased consistently resulting from the shrinkage of the Kapton HN film caused by the residual stress present in the Kapton HN film (stage II). During the cooling process (stage III), the Si NM is subjected to a compressive stress caused by the additional shrinkage of the Kapton HN film (stage III). Insets are the microscopic images of the transferred Si NM on a Kapton HN film before and after annealing at 350 °C. (b) The stress profiles as a function of time, along with temperature profile, to show the change of stress during the complete annealing process.

of 20 °C/min and annealed for 20 min. Then, the samples were cooled down to RT (25 °C) at a cooling rate of 20 °C/min. To investigate the effects of annealing temperatures on the amount of strain that can be generated, three annealing temperatures, namely, 100, 200, and 350 °C, were chosen for this study.

Raman spectroscopy (Horiba micro-Raman spectroscopy with a 532 nm wavelength laser) was used to evaluate the biaxial in-plane compressive strain in the Si NMs annealed at different temperatures. Ten areas (size: $6 \times 6 \, \mu m^2$) on the samples annealed at different temperatures, including 100, 200, and 350 °C, were randomly chosen for the characterization of in-plane compressive biaxial strains. The Si NMs were annealed for 1, 5, 10, and 20 min at 350 °C to establish the correlation between the induced compressive strain and the annealing time. The electrical current changes of the annealed Si NMs associated with their strain changes were also characterized. Raman mapping on a $100 \times 100 \, \mu m^2$ area was also performed to analyze the strain distribution. X-ray diffraction (XRD, PANalytical X'Pert PRO X-ray diffractometer) analyses were carried out for the Si NM annealed at 350 °C to evaluate the out-of-plane (perpendicular to the Si NM) strain, created by the in-plane stress. A $\theta/2\theta$ scan was taken around the (004) reflection to obtain the out-of-plane strain of the Si NM (Cu, Ka: 0.154 nm wavelength). Furthermore, in order to analyze the strain distribution in the Si NM, numerical simulations of the three-dimensional (3-D) deformation of the Si NM on the Kapton HN film were carried out by COMSOL Multiphysics.

As shown in Figure 1(b), the mechanism of the strain creation in the Si NMs is explained by the expansion and shrinkage of its substrate (i.e., the Kapton HN film) induced during the complete annealing process (i.e., the heating-annealing-cooling process). This mechanistic model was built upon COMSOL Multiphysics simulation (i.e., assuming zero net change in strain from the heating and cooling processes since the same heating and cooling rates were used.) as well as the experimental data (i.e., the measured compressive strain in the Si NM) discussed in detail below. It was reported from the manufacturer's material data sheet that a 125 μm thick Kapton HN film shrunk 0.25% and 1.54% after being annealed at 150 °C for 30 min, and 400 °C for 120 min, respectively.[12] This unique thermal property exhibited by the Kapton HN film leads to the formation of compressive strain in the Si NMs transferred onto the Kapton HN films after the complete annealing process. As shown in Figure 1(a), (1) during the temperature ramp-up stage (i.e., the heating process), the Kapton HN film expands linearly with the annealing temperature because the annealing temperature in this study is set to be below the glass transition temperature of the Kapton HN film ($T_g = 360$–410 °C) (stage I in Figure 1(b)).[12] (2) During the annealing stage when the film is heated at a constant temperature, the Kapton HN film shrinks due to the residual stress present in the Kapton HN film (stage II in Figure 1(b)). The higher is the annealing temperature, the more shrinkage occurs, and thus the desired amounts of strain can be programmed by adjusting the annealing temperature. (3) During the temperature ramp-down stage (i.e., the cooling process) (stage III in Figure 1(b)), the Kapton HN film shrinks down further. Since the heating rate and cooling rate were controlled to be the same (i.e., 20 °C/min), the total amount of expansion experienced by the Kapton HN film during the heating process and the total amount of shrinkage occurred during the cooling process cancels out. Therefore, the dimension of the Kapton HN film after the complete heating-annealing-cooling process becomes smaller than its original dimension purely due to the residual (built-in) stress present in the Kapton HN film generated during its fabrication process.[12] As shown in a Figure 1(b), the Kapton HN film experiences compressive stress after being cooled to room temperature (RT) and this compressive stress is naturally transferred to the Si NM layer. Moreover, the amount of shrinkage is dependent on the annealing temperature. Therefore, the amount of compressive strain in the Si NMs can be conveniently regulated by controlling the annealing temperature during the complete annealing process. It should be noted that the SU-8 layer experiences shrinkage after the complete annealing process[15] and this facilitates the formation of the compressive strain in Si NM. The maximum annealing temperature was still lower than the decomposition temperature (i.e., ~380 °C) of the SU-8 layer.[15] Thus, the SU-8 layer was intact within the range of annealing temperatures we studied and it functioned well as an intermediate layer for strain transfer from the Kapton HN film to the Si NM. Figure 1(a) contains two microscopic images of the transferred Si NM taken before and after it was annealed at 350 °C. No wrinkles or fractures on the strained NM were observed.

Figure 2(a) shows the typical Raman spectra of the as-transferred Si NM (i.e., without any external strains) as well as the Si NM after it was annealed at 350 °C for 20 min. The
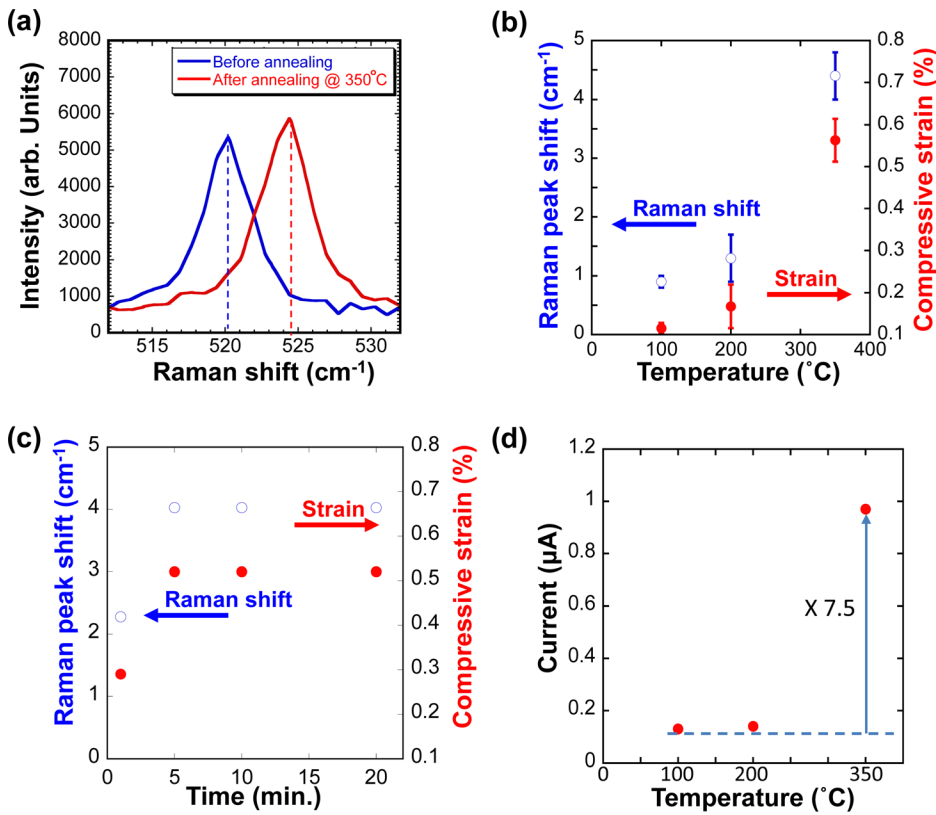
FIG. 2. (a) Raman spectra for the Si NM before and after being annealed at 350 °C for 20 min. (b) Raman peak shift (cm^{-1}) and strain (%) in the Si NM with respect to the annealing temperature (°C). (c) Raman peak shift (cm^{-1}) and strain (%) in the Si NM annealed at 350 °C with respect to the annealing time (min). (d) Current (μA) measured at 2 V between two metal electrodes on the Si NMs annealed at 100 °C, 200 °C, and 350 °C.

Raman scattering peak of the Si-Si vibration modes for the as-transferred Si NM appeared at 520.1 cm^{-1}. The Raman peak of the annealed Si NM was shifted to a larger wavenumber by 4.2 cm^{-1} compared to that of the as-transferred Si NM, indicating that a compressive strain was induced by the complete annealing process.

The biaxial stress value in the Si NM can be extracted according to the Raman shift using the following equation:[16]

$$\sigma_{xx} + \sigma_{yy}(\mathrm{MPa}) = -434 \times \Delta\omega(\mathrm{cm}^{-1}), \qquad (1)$$

where σ_{xx} and σ_{yy} are biaxial stress along the in-plane horizontal (x) and longitudinal (y) directions, respectively, and $\Delta\omega$ is the Raman peak shift. The proportional constant for Si used in Eq. (1) was calculated based on the phonon deformation potentials of Si.[17] Because the Kapton HN film has the same amount of thermal shrinkage along the x and y directions, Eq. (1) can be re-written as

$$\sigma_{xx}(\mathrm{MPa}) = \sigma_{yy}(\mathrm{MPa}) = -217 \times \Delta\omega(\mathrm{cm}^{-1}). \qquad (2)$$

The corresponding strain in the Si NM can be calculated based on the relationship among the stress (σ), strain ($\varepsilon = \sigma/E$), and Young's modulus for Si ($E_{[110]} = 169$ GPa)[18]

$$\varepsilon_{xx}(\%) = \varepsilon_{yy}(\%) = -0.128 \times \Delta\omega(\mathrm{cm}^{-1}). \qquad (3)$$

Using Eqs. (1)–(3), the biaxial strains of 0.11%, 0.16%, and 0.54% in the Si NM were calculated from the samples annealed at 100, 200, and 350 °C, respectively. Figure 2(b) shows the typical Raman peak shifts taken from 10 small areas (6×6 μm^2) on the Si NMs annealed at 100, 200, and 350 °C, respectively. Figure 2(b) shows that the induced biaxial compressive strains increased sharply against the

annealing temperatures. This behavior could be attributed to the different amount of shrinkage experienced by the Kapton HN film at different annealing temperatures.

In order to establish the correlation between the induced compressive strain and the annealing time, Raman analysis was carried out on the samples (Kapton HN film/SU-8/Si NM stack) annealed for 1, 5, 10, and 20 min at 350 °C. Figure 2(c) shows the Raman peak shift and the corresponding strain in the Si NM annealed at 350 °C at four different annealing times. The Raman peak shifts corresponding to 1, 5, 10, and 20 min annealing time were measured to be 2.28, 4.2, 4.2, and 4.2 cm^{-1}, which was converted to a compressive strain value of 0.29%, 0.54%, 0.54%, and 0.54%, respectively. Namely, according to the Raman shifts, the compressive strain reached a plateau of 0.54% within the first 5 min of the annealing process. These results indicate that the strain was induced within a short period of time during the annealing process and no strain relaxation in the Si NM was observed after 20 min annealing.

In order to determine the correlationship between the current changes and the magnitude of induced strains, two metal electrodes (Ti/Au = 20/130 nm) that were 30 μm apart were deposited onto the surface of the strained Si NM by e-beam evaporation. Figure 2(d) shows the currents measured at 2 V between the two metal electrodes for samples annealed at various temperatures. While the current changes were rather small for the samples annealed at 100 °C (0.13 μA) and 200 °C (0.14 μA), respectively, a significant current increment was observed for the sample annealed at 350 °C (0.97 μA). As demonstrated in Figures 2(b) and 2(d), the correlation between the current increase and the annealing temperature was similar to the correlation between the induced strain and the annealing temperatures. The increase

in current at high annealing temperatures could be attributed to the fact that the conduction band of Si was split into two valleys due to the presence of induced strain which consequently increased the hole mobility. Based on the calculation of the hole mobility in biaxially strained Si,[19] an approximately 50% increase in the hole mobility is expected. These results confirmed a strong correlation between the current increase and the induced strain.

Figure 3 shows that the XRD peak of Si NMs was shifted to a smaller angle after the completion of the annealing process (i.e., 350 °C). To extract the out-of-plane strain value of the Si NM from the measured XRD data, the lattice spacing needs to be calculated. Because in-plane compressive stress existed in the annealed Si NM, the lattice spacing perpendicular to the Si NM increased as the XRD peak shifted to a smaller diffraction angle. The lattice spacing normal to the top surface of the Si NM can be calculated by Bragg's law[20]

$$a = \frac{\lambda}{2 \times \sin\theta} \times \sqrt{(h^2 + k^2 + l^2)}, \quad (4)$$

where a is the lattice spacing, λ is the X-ray wavelength, θ is the diffraction angle, and (hkl) is the diffraction plane. While the full width at half maximum (FWHM) values remained the same at ∼0.04°, the diffraction angle of Si NM was shifted from 34.78° to 34.64° after the NM was annealed at 350 °C for 20 min. Accordingly, the change in lattice spacing (Δa) was calculated to be 0.01908 Å according to Eq. (4). The strain corresponding to the lattice space change can be expressed as

$$\varepsilon = \frac{\Delta a}{a}. \quad (5)$$

Based on the above equations and measurements, the tensile strain perpendicular to the Si NM was determined to be 0.35%. It should be noted that this strain value calculated from the XRD data refers to the out-of-plane strain (i.e., perpendicular to the surface), whereas the strain value of 0.54% calculated from the Raman spectrum refers to the in-plane strain (i.e., parallel to the surface).
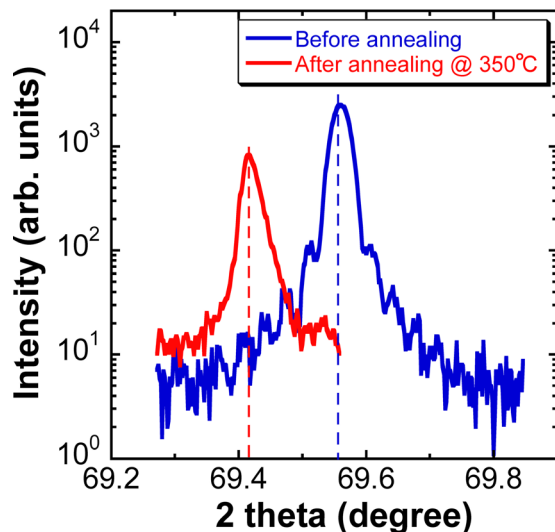

FIG. 3. X-ray diffraction (XRD) $\theta/2\theta$ spectra for the as-transferred Si NM (blue) and the Si NM after being annealed at 350 °C for 20 min (red).

In order to fully characterize the uniformity of its strain distribution in the Si NM annealed at 350 °C, a $100 \times 100\ \mu m^2$ area was scanned with a resolution of about $6 \times 6\ \mu m^2$ for the sample. Figures 4(a) and 4(b) show the Raman mapping and its corresponding Raman peaks. The highest Raman peak shift observed from area (iii) was $3.97\ cm^{-1}$ and the lowest one from area (i) was $1.75\ cm^{-1}$. In particular, the Raman peaks of the Si-Si vibrational modes of area (i), (ii), and (iii) were measured at 521.85, 523.18, and $524.3\ cm^{-1}$ which corresponded to the strain of 0.22%, 0.39%, and 0.54%, respectively. The four etched holes in the Si NM appeared as four white squares, due to the absence of Si. Although there were some minor color difference right next to the etched holes in the Raman map (referred to as the edge effect), most areas exhibit brown color. The brown color in the Raman map of the scanned areas represents the Raman peaks with a value around $524\ cm^{-1}$. The measured strain values of most areas were calculated to be 0.4%–0.5%. This uniform color distribution in the Raman map indicates that the strain was evenly distributed over a large area with a minor edge effect.

A static strain simulation was carried out by COMSOL Multiphysics with a solid stress strain model of structure mechanics to evaluate the strain distribution. Vertically stacked films of Si NM/SU-8/Kapton HN film with a surface size of $100 \times 100\ \mu m^2$ and containing four etched holes was used. The thicknesses of the Si NM, SU-8, and Kapton HN film used in the modeling were 200 nm, 1 μm, and 125 μm, respectively, which was the same with the dimensions of the samples used for the measurements. For the Si NM, Young's modulus of 169 GPa, Poisson's ratio of 0.27, and mass density of 2330 kg/m^3 were taken from literature.[21,22] Young's modulus of 2.3 and 2.5 GPa, Poisson's ratio of 0.26 and 0.34, and mass density of 1190 and 1420 kg/m^3 were used for SU-8 and Kapton HN film, respectively.[12,23,24] Based on the experimental results (i.e., the biaxial compressive strain of 0.54% in the Si NM was induced by the annealing at 350 °C), a 0.54% of shrinkage was applied on the Si NM along the x and y directions, respectively, in the simulation. Figure 4(c) shows the simulation result of the strain distribution in the Si NM. The uniform blue color indicates that the strain was evenly distributed in most part of the Si NM; however, there was a minor edge effect around the etched holes, which is consistent with the Raman map. Figure 4(d) plots the simulated strain values of the two cross-sections along a horizontal direction. The first line (line I) scans the center of the Si NM and the second line (line II) scans the regions close to the edges of the etched holes (i.e., 2 μm above the edges). As shown in the first line scan, the strain near the edges of the $100 \times 100\ \mu m^2$ Si NM was approximately 0.05% lower than the central area. The second scan shows that the strain values slightly decreased (∼0.03%) at the edges of the etched holes. Overall, the simulated strain distribution agreed well with the experimental results deduced by Raman mapping, namely, the compressive strain in the Si NM was rather uniform except the minor edge effect. For the Raman map shown in Figure 4(a), the minor edge effect was only observed at areas surrounding the etched holes, but not around the edges of the scanned region (i.e., $100 \times 100\ \mu m^2$) because the scanned Si NM was a part of the large transferred Si NM.
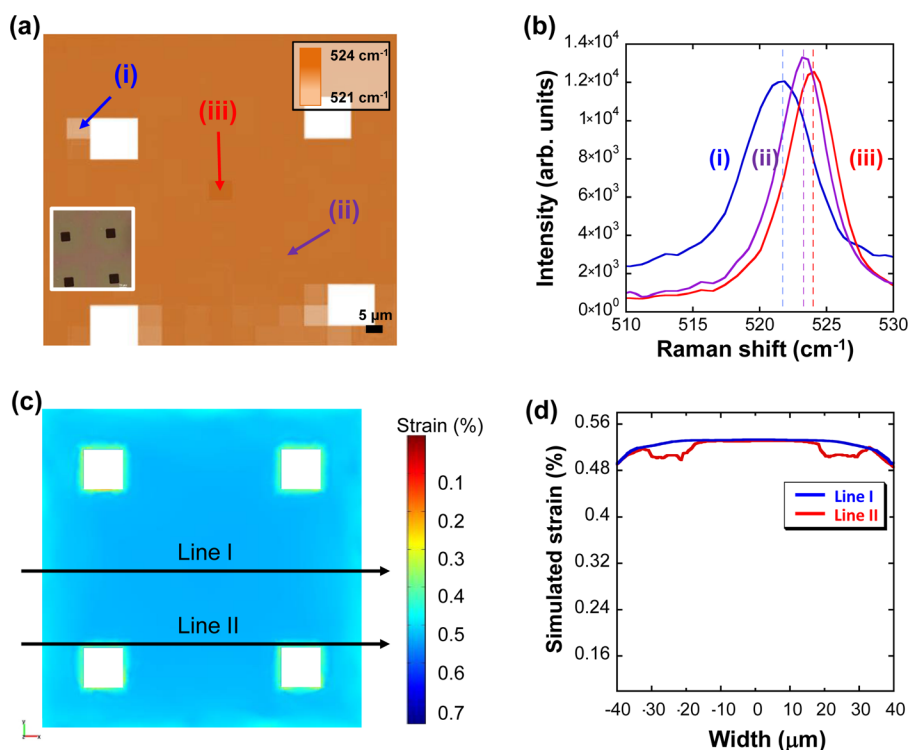
FIG. 4. (a) Raman map covering a $100 \times 100\ \mu m^2$ size after being annealed at $350\,°C$. The size of each square area is $6 \times 6\ \mu m^2$. Inset is the microscopic image of the scanned area. (b) Raman peak shifts, corresponding to the areas ($6 \times 6\ \mu m^2$) labeled as (i)–(iii) in (a). Simulated biaxial compressive strain in the Si NM transferred onto the Kapton HN film by COMSOL Multiphysics after the complete annealing process ($350\,°C$ for $20\,min$). (c) The simulated strain distribution in the Si NM transferred on the Kapton HN film. (d) The simulated strain values scanned along the lines I and II.

In summary, a simple and viable method to create programmable biaxial in-plane compressive strain in Si NM was developed using the unique thermal characteristic of the Kapton HN film. According to the Raman spectroscopy and COMSOL Multiphysics simulation, the compressive strain created in the Si NM was distributed uniformly across the NM except the minor edge effect. Within the range of annealing temperatures studied (from 100 to $350\,°C$), the amount of compressive strain created in the Si NM increased with the annealing temperatures. For instance, 0.11% and 0.54% compressive strain were generated in the Si NM at an annealing temperature of 100 and $350\,°C$, respectively. Thus, this method provides a viable approach to produce in-plane compressive strain in NMs for various applications.

[1] J. Suh, R. Nakane, N. Taoka, M. Takenaka, and S. Takagi, Appl. Phys. Lett. **99**, 142108 (2011).

[2] K. Ghosh, S. Das, A. Fissel, H. J. Osten, and A. Laha, Appl. Phys. Lett. **103**, 153501 (2013).

[3] S. Suthram, P. Majhi, G. Sun, P. Kalra, H. R. Harris, K. J. Choi, D. Heh, J. Oh, D. Kelly, R. Choi *et al.*, IEDM Tech. Dig. **2007**, 727–730.

[4] J.-P. Han, H. Utomo, L. W. Teo, N. Rovedo, Z. Luo, R. Krishnasamy, R. Stierstorfer, Y. F. Chong, S. Fang, H. Ng *et al.*, IEDM Tech. Dig. **2006**, 1–4.

[5] T. Ghani, M. Armstrong, C. Auth, M. Bost, P. Charvat, G. Glass, T. Hoffiann, K. Johnson, C. Kenyon, J. Klaus *et al.*, IEDM Tech. Dig. **2003**, 11.6.1–11.6.3.

[6] M. Segev-Bar and H. Haick, ACS Nano **7**(10), 8366–8378 (2013).

[7] M. Segev Bar, G. Konvalina, and H. Haick, Adv. Mater. **27**, 1779–1784 (2015).

[8] M. M. Roberts, L. J. Klein, D. E. Savage, K. A. Slinker, M. Friesen, Ge. Celler, M. A. Eriksson, and M. G. Lagally, Nat. Mater. **5**, 388–393 (2006).

[9] H.-C. Yuan, Z. Ma, M. M. Roberts, D. E. Savage, and M. G. Lagally, J. Appl. Phys. **100**, 013708 (2006).

[10] H. Zhou, J.-H. Seo, D. M. Paskiewicz, Y. Zhu, G. K. Celler, P. M. Voyles, W. Zhou, M. G. Lagally, and Z. Ma, Sci. Rep. **3**, 1291 (2013).

[11] J. R. Sanchez-Perez, C. Boztug, F. Chen, F. F. Sudradjat, D. M. Paskiewicz, R. B. Jacobson, M. G. Lagally, and R. Paiella, Proc. Natl. Acad. Sci. U. S. A. **108**(47), 18893–18898 (2011).

[12] See http://www2.dupont.com/Kapton/en_US/assets/downloads/pdf/HN_datasheet.pdf, for Physical properties and dimensional stability of HN Kapton film.

[13] W. Zhou, D. Zhao, Y.-C. Shuai, H. Yang, S. Chuwongin, A. Chadha, J.-H. Seo, K. X. Wang, V. Liu, Z. Ma, and S. Fan, Prog. Quantum. Electron. **38**(1), 1–74 (2014).

[14] S.-W. Youn, A. Ueno, M. Takahashi, and R. Maeda, Microelectron. Eng. **85**, 1924–1931 (2008).

[15] R. Feng and R. J. Farris, J. Micromech. Microeng. **13**, 80–88 (2003).

[16] I. D. Wolf, J. Raman Spectrosc. **30**, 877–883 (1999).

[17] E. Anastassakis, A. Cantereo, and M. Cardona, Phys. Rev. B **41**, 7529–7535 (1990).

[18] C. Himcinschi, M. Reiche, R. Scholz, S. H. Christiansen, and U. Gosele, Appl. Phys. Lett. **90**, 231909 (2007).

[19] D. Yu, Y. Zhang, and F. Liu, Phys. Rev. B **78**, 245204 (2008).

[20] C. Kittel and P. McEuen, *Introduction to Solid State Physics,* 8th ed. (John Wiley & Sons Inc., 2004).

[21] J. J. Wortman and R. A. Evans, J. Appl. Phys. **36**, 153 (1965).

[22] L. B. Freund and S. Suresh, *Thin Film Materials: Stress, Defect Formation, and Surface Evolution* (Cambridge University Press, Cambridge, UK; New York, 2003).

[23] S. Keller, G. Blagoi, M. Lillemose, D. Haefliger, and A. Boisen, J. Micromech. Microeng. **18**, 125020 (2008).

[24] I. Roch, P. Bidaud, D. Collard, and L. Buchaillot, J. Micromech. Microeng. **13**, 330–336 (2003).